


Article

Thermodynamic Analysis of Pumped Thermal Energy Storage System Combined Cold, Heat, and Power Generation

Yijing Wang ¹, Yonggao Yin ^{1,*}, Zhanxiao Kang ²  and Jintu Fan ²¹ School of Energy and Environment, Southeast University, Nanjing 210096, China; wangyijing2001@163.com² School of Fashion and Textiles, The Hong Kong Polytechnic University, Hong Kong 999077, China; z.x.kang@polyu.edu.hk (Z.K.); jin-tu.fan@polyu.edu.hk (J.F.)

* Correspondence: y.yin@seu.edu.cn

Abstract: Aiming at problems such as the low efficiency of renewable energy conversion and the single energy flow mode, this paper proposes a heat pump energy storage system combining cold, heat and power generation to achieve the purpose of diversified utilization of renewable energy. The system is suitable for buildings requiring cooling, heating/domestic hot water production and electricity. This paper mainly uses MATLAB for numerical calculations, selects several key cycle parameters to calculate and analyze the thermodynamic performance of the system, and uses the genetic algorithm and TOPSIS decision method to carry out fine design of the system working conditions. Through the multi-objective optimization calculation and the optimal solution, the system can achieve a total energy efficiency of 2.39 and a high thermal economic performance, indicating that the system can achieve the goals of cooling, heating water and power supply and providing ideas for the application of the multiple energy storage system.

Keywords: pumped thermal energy storage; carbon dioxide heat pump; multi-energy storage; multi-objective optimization



Academic Editor: Mahmoud Bourouis

Received: 24 December 2024

Revised: 17 January 2025

Accepted: 21 January 2025

Published: 23 January 2025

Citation: Wang, Y.; Yin, Y.; Kang, Z.; Fan, J. Thermodynamic Analysis of Pumped Thermal Energy Storage System Combined Cold, Heat, and Power Generation. *Energies* **2025**, *18*, 525. <https://doi.org/10.3390/en18030525>

Copyright: © 2025 by the authors. Licensee MDPI, Basel, Switzerland. This article is an open access article distributed under the terms and conditions of the Creative Commons Attribution (CC BY) license (<https://creativecommons.org/licenses/by/4.0/>).

1. Introduction

With the strengthening of development and investment in renewable energy such as wind and solar energy, renewable energy, led by both, will become the fastest growing energy source in the world in the next 30 years [1]. However, due to the intermittent and fluctuating characteristics of renewable energy generation [2], with the increase in its penetration rate in the power grid, the grid connection of renewable energy will have some impact on the traditional power grid [3,4]. Energy storage technology is the key to the full utilization of renewable energy. Realizing the movement of energy in time and space is the key principle of energy storage [5], which is essentially to make energy more controllable. The basic principle of electricity storage technology is that the electric energy is converted into other forms of energy storage when there is excess electric energy production, and when electric demand is large, the other forms of energy stored are re-converted into electric energy and released through certain technical means to achieve the function of peak regulation of electric energy.

To fully utilize renewable energy sources, the global effort to shift away from fossil fuels calls for energy storage that is efficient, affordable, and sustainable. The Carnot battery [6,7] could revolutionize the energy storage sector [8]. Pumped thermal electricity storage (PTES) technology, also known as the “Carnot battery”, combines thermal cycle technology with energy storage technology [9] and is a new type of electricity storage technology developed in recent years. The realization of the PTES charge/discharge

function is not limited by geographical conditions and will not bring environmental and safety problems. At the same time, PTES has the advantages of large capacity, sufficient power, high efficiency, low cost, and long heat storage period [10,11]. According to the different operating principles of the system, PTES can be further divided into supercritical Brayton cycle PTES, transcritical cycle PTES, and subcritical cycle PTES.

The storage temperature of the Brayton PTES system is high, usually above 500 °C. The material and process requirements and quality of the system are high, resulting in an increase in the initial investment of the system [12]. Compared with the Brayton PTES system, there are relatively few studies on PTES based on the Rankine cycle. The transcritical cycle PTES system, such as the transcritical CO₂ PTES system, uses non-toxic, non-flammable, environmentally friendly CO₂, which has excellent thermal performance, as the working fluid because its working temperature is lower than 200 °C. As a heat/cold storage medium, pressurized water has a broad development prospect in the field of energy storage. In the transcritical CO₂ PTES system established by Mercangöz et al. [13], the heat storage system consisted of four heat storage tanks and four ice storage tanks. The results showed that the efficiency of the system reached 53%, and the maximum pressure reached 13.3 MPa when the maximum storage temperature was only 396 K. Morandin et al. [14,15] optimized different transcritical CO₂ cycle configurations using hot water and brine ice for heat and cold storage, respectively, and the cycle efficiency reached 60%. The maximum temperature of the system was only 450 K, but the maximum pressure was 18.9 MPa. In the follow-up study, Morandin et al. [16] optimized the thermal economic performance of the different system configurations they proposed. The charging and discharging power of the system was 50 MW, the charging and discharging time was 2 h, and the cycle efficiency was increased to 64%. In view of the high storage pressure of CO₂ as a working fluid, Carro et al. [17] proposed a PTES system in which high-pressure CO₂ is stored in abra. This system is suitable for different scenarios of renewable energy storage and carbon capture systems, and the storage efficiency reaches 42–56%. Combined with renewable energy storage, the system can store more than 1 Mt of additional CO₂ per year.

The application of the Rankine cycle-based PTES system in the integrated energy system is particularly important. Reference [18] designed a PTES system suitable for industrial parks. The system could integrate the low-temperature waste heat of industrial parks as the basis of electricity storage and meet the steam demand of the industrial parks at the same time. In the case of industrial parks, the steam heat PTES system has a round-trip efficiency of 55.6%, a COP of 3.3, and a heating efficiency of 68.2%, which shows to a certain extent that the heat pump energy storage system based on the Rankine cycle has considerable energy storage performance. At the same time, the high efficiency of thermoelectric conversion gives it the ability to integrate and redistribute the thermal and electrical resources [19]. Although in terms of performance, the PTES system based on the Rankine cycle has shown good competitiveness, the practical economy of the heat pump storage system is still open to question. Taking data centers as practical application scenarios, Antoine [20] explored the technical and economic potential of heat pump power storage system based on the Rankine cycle. His research idea was to improve system efficiency by recycling waste heat, thus enhancing the economy of the system.

In recent years, the development of Carnot battery technology has been rapid, and several representative research projects have been initiated, for example, the National Facility for Pumped Heat Energy Storage (Newcastle University, Cambridge, UK, 150 kW grid-scale demonstration), the CHESTER Project (EU Horizon 2020, 10 kWe lab-scale prototype system), and the Malta system (Malta, Inc., Cambridge, UK, 100 MW grid-

scale solution). Initially, the Carnot battery concept was chiefly centered around electric energy storage. However, its application scope has now expanded to multi-vector energy domains, such as combined cooling, heating, and power (CCHP). These multi-energy management systems gain enhanced flexibility and efficiency by integrating different energy sources, including solar, wind, and waste heat, and being applicable to intricate application scenarios. Take the Rankine cycle-based Carnot battery systems as an example. They are capable of making use of waste heat. Provided that waste heat is considered costless, they can theoretically reach a roundtrip efficiency exceeding 100%. Due to this advantage, they have been suggested as an approach for renovating existing coal-fired power plants, as well as solar thermal and photovoltaic (PV) power plants.

Much of the literature has focused on grid power to storage intermediates (high-temperature thermal energy), which, after a period of time, are converted back into electrical energy. However, there is a lack of research on how to convert grid power into more intermediate products. Based on the current research situation, a new concept combining the Carnot battery and multiple energy storage is proposed in this paper: power supply from the grid to the multistage heat pump, generating cold, medium-temperature heat, and high-temperature heat; the cold capacity and medium-temperature heat can be used by users, and the high-temperature heat can meet the needs of power generation. In view of the current problems of low efficiency of distributed energy conversion and the time–space mismatch between supply and demand, this kind of pumped thermal energy storage system is a viable choice for sustainable energy development in the future [21]. In this paper, the key parameters such as heat pump parameters and heat engine parameters are studied, and the performance is analyzed. The genetic algorithm is used to optimize the system. The performance calculation and analysis were completed by MATLAB R2020a.

2. System Description

This section mainly introduces the basic operation principle of the system and the system operation process.

2.1. System Principle

The principle of the multiple energy storage system based on CO₂ heat pump energy storage is shown in Figure 1. By compressing the working fluid several times, the heat is stored and utilized in steps, so as to achieve the purpose of storing renewable electricity in the form of cold and hot energy storage fluid. Unlike the conventional pumped thermal energy storage system, which stores electric energy only in the form of cold heat with a large temperature difference in the energy storage unit, the system stores about 0 °C of cold energy on the energy storage side to meet the cooling load demand on the user side. At the same time, it stores 50 °C medium-temperature hot water, which is used to provide domestic hot water for the user side, and it stores the high-temperature heat of about 115 °C for driving the turbine to generate electricity. The system not only can store renewable power, but can also realize the flexible regulation of storage/release of power and meet the demand of multiple loads of heating and cooling in different periods.

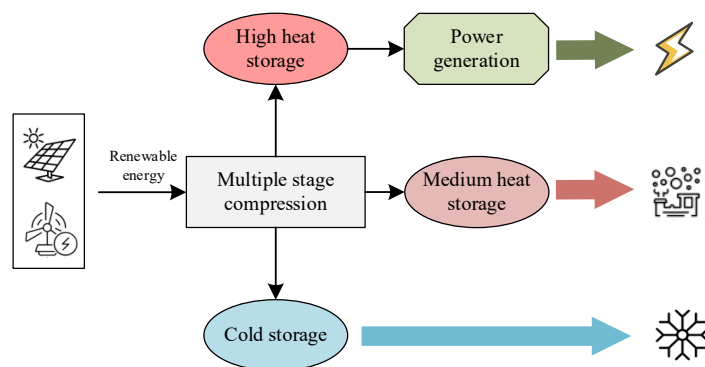


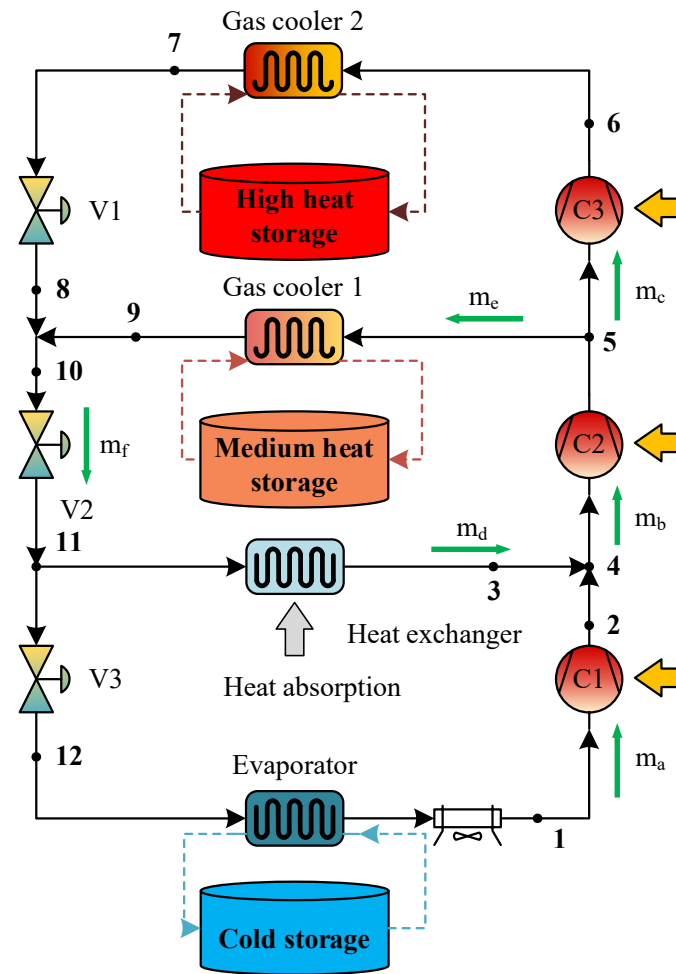
Figure 1. General description of the multiple energy storage system.

2.2. System Process

The heat pump energy storage system is mainly composed of the energy storage cycle and energy release cycle, and the main components are the compressor, heat exchanger, throttle valve, pump, and turbine.

- (1) As shown in Figure 2a, when the system performs the energy storage process, the cycle operation mode is similar to that of a multistage compression heat pump. The initial state of the working fluid of the cycle is 1. From state 1 to 2 is the first stage of compression. The low-temperature and low-pressure CO_2 (m_a) is mixed with the working fluid (m_d) after the first stage of compression (C1), becoming stage 4. From state 4 to 5 is the second stage of compression; the mixed working fluid (m_b) enters the second stage compressor (C2) to become the medium-temperature and -pressure working fluid. From state 11 to 3 is the heat equilibrium process. The heat exchanger on the m_d branch is designed to balance the heat of the system by absorbing heat from the air to achieve the thermal balance of the first stage compression circuit. From state 5 to 6 is the third stage of compression. From state 5 to 9 is the process of medium-temperature heat storage in gas cooler 1. After diverting the working fluid after the second-stage compressor, some working fluid (m_e) is heat exchanged with water in gas cooler 1 for medium-temperature heat storage ($50\text{ }^\circ\text{C}$), and the other (m_c) enters the third-stage compressor. From state 6 to 7 is the process of high-temperature heat storage in gas cooler 2. After three stages of compression, the working fluid reaches a high-temperature and high-pressure state, and this part of the high-temperature heat is stored in water through the gas cooler 2 for high-temperature heat storage ($120\text{ }^\circ\text{C}$). From state 7 to 8 is the process of throttling in throttle valve 1. From state 10 to 11 is the process of throttling in throttle valve 2. The working fluid of the outflow gas cooler is medium-temperature and high-pressure supercritical CO_2 , which enters the first-stage throttle to become the medium-temperature and medium-pressure working fluid, and then, enters the second-stage throttle after mixing (m_f) with the medium-temperature heat transfer working fluid (m_e). From state 11 to 12 is the process of throttling in throttle valve 3. From state 12 to 1 is the cooling process in the evaporator. After two throttling processes, the working fluid is divided into two ways: one way (m_d) absorbs environmental heat for heat balance, and the other way (m_a) carries out the third-stage throttling to become low-temperature and low-pressure working fluid, absorbs the heat of the coolant in the evaporator, and restores the initial state of the working fluid.
- (2) As shown in Figure 2b, the energy release process is the heat engine cycle. From state a to b is the pressurization process in the pump. The low-temperature, low-pressure working fluid (m_t) is pressurized by the pump to become the low-temperature, high-pressure working fluid. From state b to c is the heating process in the recuperator.

The low-temperature working fluid at state b of the recuperator is exchanged with the waste heat at the turbine outlet. From state c to d is the heating process in the gas heater. From state d to e is the expansion process of the turbine. The working fluid flows into the gas heater and uses the high-temperature heat stored in the energy storage cycle to heat the working fluid, thus becoming the high-temperature, high-pressure supercritical CO₂ in the turbine expansion power generation. From state f to a is the cooling process in the condenser. The medium-temperature fluid at the turbine outlet can preheat the working fluid at the outlet of the pump, and the CO₂ after heat exchange can further release excess heat to the environment and return to the initial state.

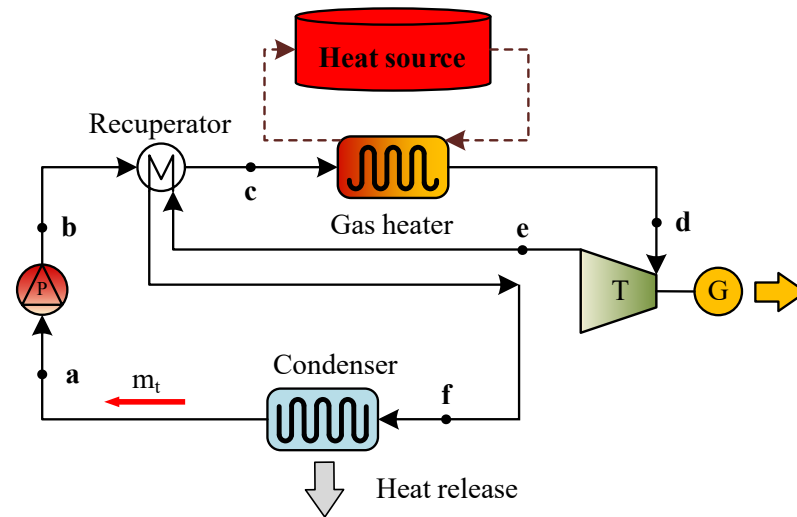


C1, C2, C3- Compressor; V1, V2, V3- Throttle valve
m- Mass flow rate

1-C1 inlet; 2-C1 outlet; 3-Heat exchanger outlet; 4-
C2 inlet; 5-C2 outlet; 6-C3 outlet; 7-Gas cooler 2
outlet; 8-V1 outlet; 9-Gas cooler 1 outlet; 10-V2
inlet; 11-V2 outlet; 12-V3 outlet.

(a)

Figure 2. Cont.



P- Pump; T- Turbine; G- Generator

a-Pump inlet; b-Pump outlet; c-Recuperator outlet; d-Gas heater outlet; e-Turbine outlet; f-Condenser inlet.

(b)

Figure 2. Schematic diagram of multiple energy storage system. (a) Schematic diagram of energy storage cycle. (b) Schematic diagram of energy release cycle.

3. Materials and Methods

This section mainly introduces the modeling of the system, models the various components of the system, establishes the performance index of the system, and finally, verifies the validity of the model.

3.1. Mathematical Models

In order to study the thermodynamic performance of the PTES system, it is necessary to establish the thermodynamic model of the main components of the system in order to analyze the overall thermodynamic performance of the system. In the process of building the thermodynamic model of the system, in order to simplify the calculation and analysis process, the following basic assumptions are made:

- (1) The system is in a stable operation state and does not consider the specific heat transfer process;
- (2) The heat transfer loss between the internal and external pipes and compressors and the external environment is ignored;
- (3) The pressure drop of CO₂ and energy storage medium in the flow process is ignored, and the flow rate and temperature are evenly distributed;
- (4) Mass conservation is satisfied at each part of the system; that is, the outlet flow of the connected component is equal to the inlet mass of the next component.

3.1.1. Heat Pump Modeling

The working fluid is pressurized in the compressor, and the calculation methods of the isentropic efficiency of the compressor are shown in Equation (1):

$$\eta_{is,com1} = \frac{h_{2s} - h_1}{h_2 - h_1}; \eta_{is,com2} = \frac{h_{5s} - h_4}{h_5 - h_4}; \eta_{is,com3} = \frac{h_{6s} - h_5}{h_6 - h_5} \quad (1)$$

where the subscript “is” indicates isentropic, and the numbers in the subscripts represent different state points.

The input work of each stage compressor is shown in Equation (2):

$$W_{C1} = m_a \times (h_2 - h_1); W_{C2} = m_b \times (h_5 - h_4); W_{C3} = m_c \times (h_6 - h_5) \quad (2)$$

where m_a , m_b , and m_c are, respectively, the mass flow rates of the first-, second-, and third-stage compressors.

In the throttle model, the specific enthalpy of the working fluid at the inlet and outlet is the same, and the calculation method is shown in Equation (3):

$$h_7 = h_8; h_{10} = h_{11}; h_{11} = h_{12} \quad (3)$$

In this paper, all the heat exchangers in the system are tube-in-tube heat exchangers. The energy conservation equation of each heat exchanger is shown in Equation (4):

$$m_c \times (h_{c,o} - h_{c,i}) = m_w \times (h_{w,i} - h_{w,o}) \quad (4)$$

where m_c and m_w are, respectively, the mass flow rate of working fluid and heat storage fluid; $h_{c,o}$ and $h_{w,o}$ are, respectively, the outlet specific enthalpy of working fluid and heat storage fluid; $h_{c,i}$ and $h_{w,i}$ are, respectively, the inlet specific enthalpy of working fluid and heat storage fluid.

3.1.2. Heat Engine Modeling

According to the theory of heat transfer and engineering thermodynamics, the process of working medium pump doing work to working medium is an adiabatic process, and the calculation method of adiabatic efficiency is shown in Equation (5):

$$\eta_{is,p} = \frac{h_{bs} - h_a}{h_b - h_a} \quad (5)$$

The output work of pump is shown in Equation (6):

$$W_p = m_t \times (h_b - h_a) \quad (6)$$

where m_t is the mass flow rate of heat engine cycle.

According to the theory of heat transfer and engineering thermodynamics, the expansion process in a turbine is an adiabatic process, and the calculation method of adiabatic efficiency is shown in Equation (7):

$$\eta_{is,t} = \frac{h_d - h_e}{h_d - h_{es}} \quad (7)$$

The output work of the turbine is shown in Equation (8):

$$W_T = m_t \times (h_e - h_d) \quad (8)$$

3.1.3. Energy Balance Equations and Other Correlations

The calculation method of cold storage capacity Q_{cold} is shown in Equation (9):

$$Q_{cold} = m_a \times (h_1 - h_{12}) \quad (9)$$

The calculation method of heat storage at medium temperature $Q_{hot,m}$ is shown in Equation (10):

$$Q_{hot,m} = m_e \times (h_5 - h_9) \quad (10)$$

where m_e is the mass flow rate of working fluid in gas cooler 1.

The calculation method of heat storage at high temperature $Q_{hot,h}$ is shown in Equation (11):

$$Q_{hot,h} = m_c \times (h_6 - h_7) \quad (11)$$

The input work and calculation method of the first-, second-, and third-stage compressors W_{C1}, W_{C2}, W_{C3} is shown in Equation (12):

$$W_{C1} = m_a \times (h_2 - h_1); W_{C2} = m_b \times (h_5 - h_4); W_{C3} = m_c \times (h_6 - h_5) \quad (12)$$

The calculation method of total input energy W_C is shown in Equation (13):

$$W_C = W_{C1} + W_{C2} + W_{C3} \quad (13)$$

There is mixing of working fluid at point 4, which can be modeled by mass flow balance and energy balance, as shown in Equations (14) and (15):

$$m_a + m_d = m_b \quad (14)$$

$$m_a \times h_2 + m_d \times h_3 = m_b \times h_4 \quad (15)$$

There is mixing of working medium at point 10, which can also be modeled by mass flow balance and energy balance, as shown in Equations (16) and (17),

$$m_c + m_e = m_f \quad (16)$$

$$m_c \times h_8 + m_e \times h_9 = m_f \times h_{10} \quad (17)$$

where m_f is the mass flow rate of working fluid in throttle valve 2.

By combining the mass flow balance at point 11 and point 4, Equation (18) can be obtained:

$$m_f = m_b \quad (18)$$

The calculation method of heat transfer of gas heater is shown in Equation (19):

$$Q_h = m_t \times (h_d - h_c) \quad (19)$$

The power output of the heat engine cycle W_{out} is obtained by subtracting the power consumption of the pump from the output work of the turbine, and the calculation equation is shown in Equation (20):

$$W_{out} = m_t \times (h_d - h_e - h_b + h_a) \quad (20)$$

The heat balance equation of the regenerator is shown in Equation (21):

$$h_c - h_b = h_e + h_f \quad (21)$$

The efficiency of the heat engine cycle can be calculated by Equation (22):

$$\eta_{he} = \frac{W_{out}}{Q_h} \quad (22)$$

3.2. Thermodynamic Performance Evaluation Indexes

In this article, two performance indexes related to the thermodynamic performance and thermal economic performance of the system are established, and their specific meanings are shown as follows.

3.2.1. Energy Efficiency

The performance coefficient of the CO₂ pumped thermal energy storage cycle in this paper can be compared with that of the conventional heat pump system. Since the energy efficiency in this article mainly focuses on the conversion and utilization efficiency of electric energy, and it focuses on the energy utilization capacity in the system process of electric energy storage and release, the power consumed by pumping the working medium and heat storage fluid is ignored. The ability to convert electrical energy into electricity and heat and cold energy is the ability of energy utilization to measure the comprehensive thermal performance of the system. It is defined as the ratio of the sum of the cold storage capacity of the heat pump, the medium-temperature heat storage capacity, and the net electric energy of the heat engine cycle output system to the total electric energy of the heat pump cycle input system through the compressor, as shown in Equation (23):

$$\eta_{all} = \frac{Q_{cold} + Q_{hot,m} + W_{out}}{W_C} \quad (23)$$

3.2.2. Total UA Value

When calculating the thermal economic performance of the heat exchanger, the UA value is usually used to represent the product of the heat transfer area and the total heat transfer coefficient. Therefore, the UA value can also be interpreted as heat exchanger performance. For the same fluid, when the heat exchanger model is determined, the total heat transfer coefficient is basically determined. The greater the UA value of the heat exchanger, the greater the heat exchange area required, the higher the cost of heat storage, and the higher the cost of the heat exchanger [22]. This paper defines the total UA value of the heat pump/heat engine cycle, which is the sum of the UA values of the heat exchanger in the charge/discharge cycle. The specific calculation equation is shown in Equation (24):

$$UA_{all} = UA_{hp} + UA_{he} \quad (24)$$

Taking the heat pump cycle heat storage process as an example, the calculation equation of the logarithmic mean temperature difference in the heat transfer process is shown in Equation (25).

It should be noted that the logarithmic mean temperature difference here refers to the temperature difference between the working fluid and the heat-storage fluid in the gas cooler and gas heater, and the value of the logarithmic mean temperature difference depends on the inlet and outlet temperatures of the working fluid and heat-storage fluid. For the heat-transfer process in the evaporator, because it is an isothermal process, the initial value of the heat transfer temperature difference is set to 5 °C.

$$\Delta T_{hot} = \frac{(T_{ci} - T_{wo}) - (T_{co} - T_{wi})}{\ln \frac{T_{ci} - T_{wo}}{T_{co} - T_{wi}}} \quad (25)$$

The equation for calculating the UA value of each heat exchanger is shown in Equation (26):

$$UA = Q / \Delta T_{hot} \quad (26)$$

3.3. Model Validation

Based on the thermodynamic model built in this section and combined with the design parameters of each component in reference [23], the operating parameters of the system components in the literature were validated. The specific design parameters and values of the system in [23] are shown in Table 1. Table 2 shows the model validation results of the system. The error analysis index in the process of model verification is relative error x , and its calculation method is shown in Equation (27) [24]:

$$x = \frac{\text{Calculation values} - \text{Reference values}}{\text{Reference values}} \quad (27)$$

Table 1. System design parameters of the literature.

Parameter	Physical Meaning	Value
$P_{hp,l}$	Low pressure of heat pump	1.8 MPa
$P_{hp,h}$	High pressure of heat pump	12.2 MPa
T_{com}	Inlet temperature of compressor	9.7 °C
T_{out}	Outlet temperature of gas cooler	5.6 °C
$P_{he,l}$	Low pressure of heat engine	2.1 MPa
$P_{he,h}$	High pressure of heat engine	14.4 MPa
T_{turb}	Inlet temperature of turbine	175.8 °C

Table 2. Relative error in system model validation.

Parameter	Calculated Value	Reference Value	Relative Error
Power consumption of compressor	132.12 kW	130.6 kW	1.2%
Output work of turbine	95.24 kW	99.4 kW	−4.2%
Power consumption of pump	17.36 kW	16.8 kW	3.3%
Heat storage by heat pump	358.8 kW	352 kW	1.9%
Heat consumption of heat engine	337.36 kW	336.4 kW	0.3%

According to Table 2, based on the system model established in this section and the design parameters of the literature, the relative error of output work of the turbine in each parameter of the system is the maximum of −4.2%, and the relative error of all parameters is less than 5%. The above data show that the calculation error of the model established in this paper is relatively small, and the calculation results of the model are acceptable.

4. Results and Discussion

The thermodynamic performance of the PTES system depends on the design parameters of the heat pump and the heat engine, so the design parameters of the heat pump and the heat engine should be considered comprehensively when evaluating the thermodynamic performance of the system. In all key design parameters of the heat pump and heat engine, four sets of design parameters are considered according to the operation characteristics of bidirectional conversion, and the thermodynamic performance of different sets of design parameters is comprehensively analyzed and evaluated. This section uses the evaluation indicators proposed in Section 3.2 as the basis, and when one set of parameters is investigated, the other parameters retain the default values shown in Table 3 and the influence law of the system's thermal performance with the changes of the following four groups of key parameters. The thermophysical properties of the working fluid were obtained by using REFPROP v9.1 software developed by NIST in MATLAB.

Table 3. Main parameters and values.

Parameter	Physical Meaning	Value
W_C	Total input power	100 kW
$\eta_{is,c}$	Isentropic efficiency of compressor	86%
$\eta_{is,p}$	Isentropic efficiency of pump	85%
$\eta_{is,t}$	Isentropic efficiency of turbine	88%
T_{amb}	Ambient temperature	25 °C
P_{hp}	High pressure of heat pump	12 MPa
T_{eva}	Evaporating temperature of heat pump	0 °C
$T_{hot,m}$	Medium heat storage temperature	55 °C
$T_{hot,h}$	High heat storage temperature	115 °C
T_{com}	Inlet temperature of compressor	20 °C
P_{he}	High pressure of heat engine	12 MPa
T_{cond}	Condensing temperature of heat pump	25 °C
P_{water}	Water pressure	0.5 MPa
ΔT	Heat transfer temperature difference of evaporator	5 °C
Δt_{pp}	Pinch point temperature difference	1 °C

4.1. Critical Parameters of Heat Pump

The high pressure of the heat pump P_{hp} and the evaporating temperature T_{eva} represent the key parameters of the heat pump cycle, which represents the pressure range of the heat pump cycle operation and has a significant impact on the energy storage process, so it is necessary to explore the influence of these parameters on the overall thermodynamic performance.

Figure 3 shows the results of η_{all} and UA_{all} with respect to P_{hp} and T_{eva} : η_{all} and UA_{all} decrease as P_{hp} and T_{eva} increase. This is because when P_{hp} increases, the outlet enthalpy of the compressor increases while the inlet enthalpy stays the same, and the compressor's work consumption and heat storage temperature increase. Since the heating temperature of the working medium of the heat engine cycle is affected by the heat storage temperature, the discharge energy increases, so UA_{all} decreases. On the other hand, when T_{eva} increases, the inlet enthalpy of the compressor increases while the outlet enthalpy remains unchanged, resulting in a decrease in the enthalpy difference between the inlet and outlet of the compressor, further reducing the input electrical work, but the increment of cold storage capacity is greater than the decrease in the compressor power consumption. In addition, T_{eva} does not affect the energy release cycle, which means that the output energy is unchanged, and eventually η_{all} is reduced.

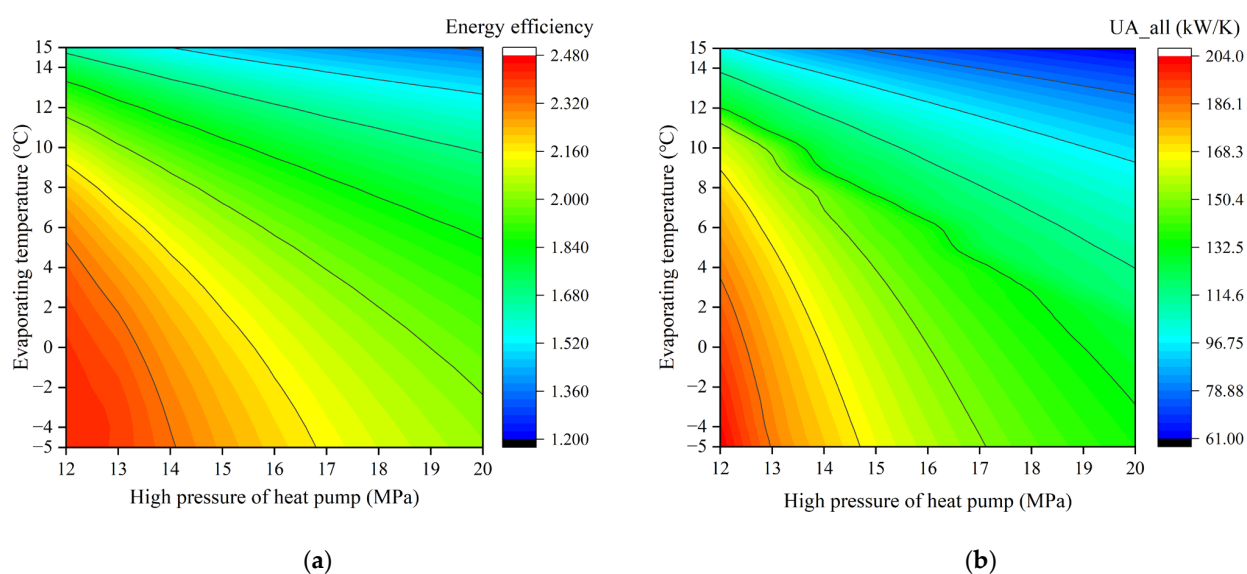


Figure 3. (a) The impact of heat pump parameters for η_{all} . (b) The impact of heat pump parameters for UA_{all} .

As shown in Figure 4, the heat storage temperature increases with the increase in the high pressure of the heat pump, but it decreases with the increase in the evaporation temperature, because although the compressor inlet enthalpy increases, the flow rate of the circulating working fluid decreases. When $P_{hp} = 12$ MPa and $T_{eva} = -5$ °C, η_{all} of the system reaches the highest value of 2.43. The change trend of UA_{all} is the same as that of η_{all} , and the minimum value of UA_{all} is 61.32 kW/K when $P_{hp} = 20$ MPa and $T_{eva} = 15$ °C are used.

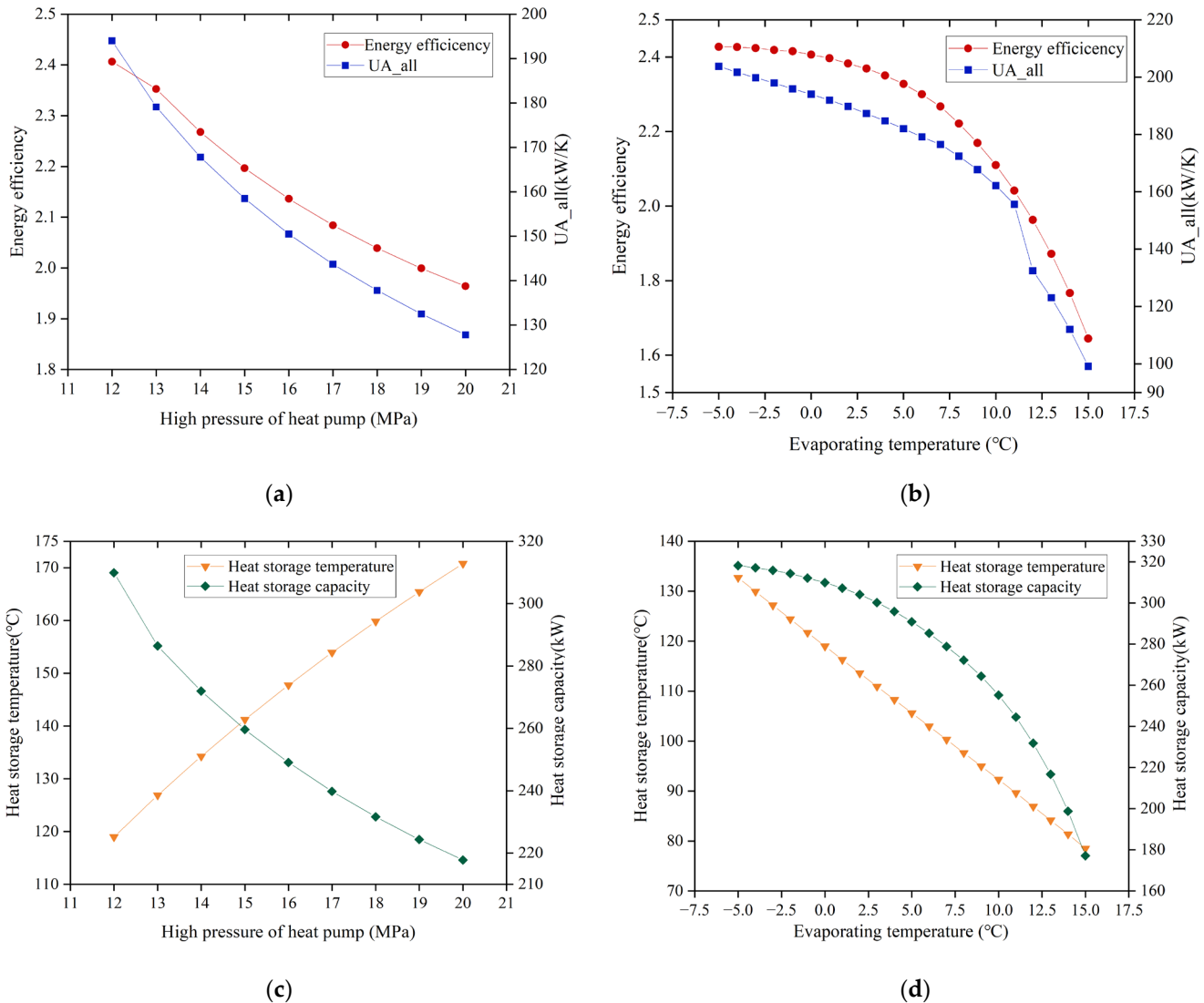


Figure 4. (a) The impact of high pressure of the heat pump on system performance; (b) the impact of evaporating temperature on system performance; (c) the impact of high pressure of the heat pump on heat storage capacity; (d) the impact of evaporating temperature on heat storage capacity.

The results show that although the system performance decreases when the heat pump pressure and evaporation temperature are increased, the economic performance of the system can be increased. It is impossible to obtain the best economic performance and the highest energy efficiency at the same time under the same working parameters, so those working parameters need to be optimized to achieve a better compromise performance.

4.2. Critical Parameters of Heat Engine

The high-pressure P_{he} and condensing temperature T_{cond} of the heat engine represent the key parameters of the heat engine cycle and reflect the pressure range of the heat engine cycle, which has a significant impact on the energy release process, so it is necessary to analyze the influence of these parameters on the overall thermodynamic performance.

Figure 5 shows the results of η_{all} and UA_{all} as a function of P_{he} and T_{cond} . It can be seen that the change in η_{all} and UA_{all} with the heat engine parameters is not simply a linear relationship. However, the rate of change in UA_{all} is less than 5%, and it can be approximated that UA_{all} changes little with P_{he} and T_{cond} . Therefore, this paper mainly studies the influence of P_{he} and T_{cond} on η_{all} . When the influences of pressure and condensing temperature are studied separately, as shown in Figure 6, when P_{he} increases, η_{all} increases slightly and then decreases, mainly because the change in P_{he} causes a decrease in turbine inlet enthalpy, which leads to a decrease in discharge, and finally makes η_{all} show a downward trend, reaching the highest value of 2.41 at approximately $P_{he} = 13.6$ MPa. With the increase in P_{he} , UA_{all} decreases slightly at first and then increases. Contrary to the change trend of η_{all} , the minimum value of UA_{all} at $P_{he} = 13.9$ MPa is 193.9 kW/K.

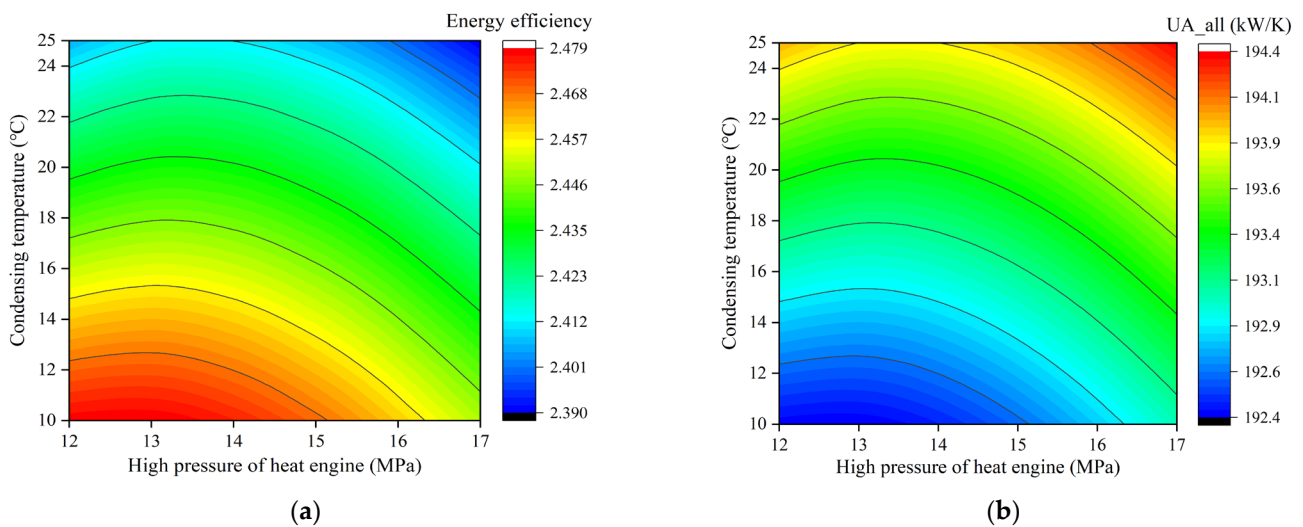


Figure 5. (a) The impact of heat engine parameters on η_{all} ; (b) the impact of heat engine parameters on UA_{all} .

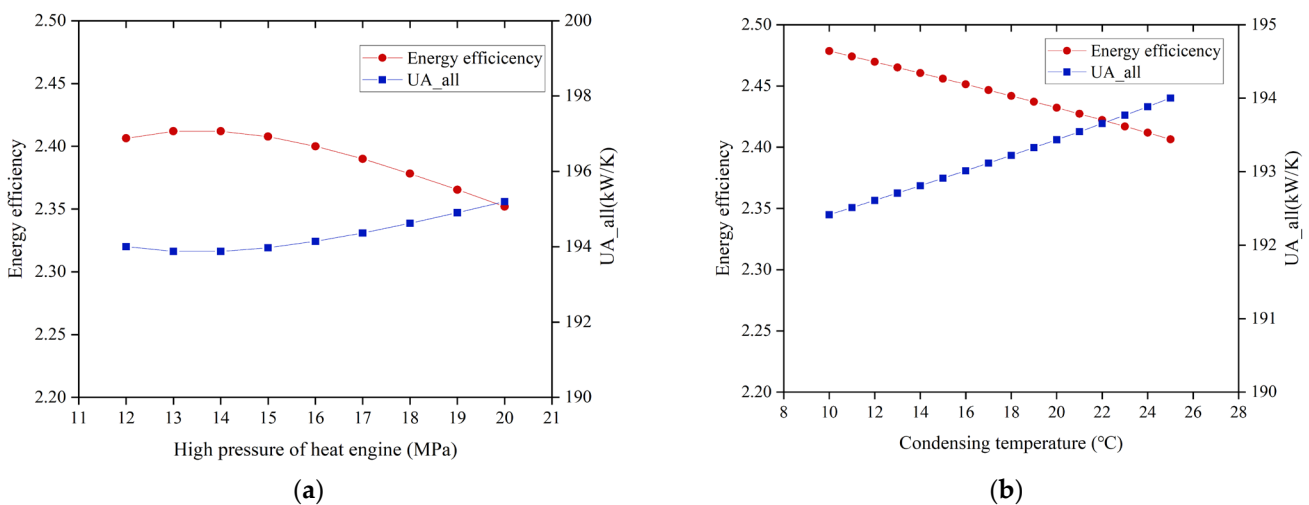


Figure 6. (a) The impact of high pressure of heat engine on system performance; (b) the impact of condensing temperature on system performance.

According to the calculation results, since the parameters of the heat pump are almost unaffected when the critical parameters of the heat engine are studied, the heat storage temperature at this stage is always 119.8 °C, and the heat storage is 310.7 kW. Although the system performance index and heat storage capacity show a nonlinear change trend with the change in the critical parameters of the heat engine, the rate of change is less than 5%, so it can be approximated that the critical parameters of the heat engine have little influence on the system performance.

4.3. Coupling Parameters of Charge/Discharge System

This set of parameters reflects the influence of heat storage temperature on the overall thermodynamic performance of the energy storage/release cycle. When the evaporating temperature is determined, the heat exchange temperature difference in the heat exchanger determines the temperature of the cold storage medium, which affects the energy utilization effect of the energy storage/release cycle. Moreover, the inlet temperature (superheat) of the compressor is also one of the key factors affecting the heat storage temperature, so it is necessary to explore the influence of these two coupling parameters on the overall thermodynamic performance.

The effects of ΔT and T_{com} on η_{all} and UA_{all} are shown in Figures 7 and 8. It can be seen that η_{all} increases with the increase in T_{com} and decreases with the increase in ΔT . UA_{all} decreases as ΔT increases but is almost unaffected by T_{com} . When T_{com} increases, the compressor outlet temperature increases, the heat storage increases, and the discharge power also increases, so the energy efficiency increases. When ΔT increases, the cold storage temperature increases and the heat storage temperature decreases, resulting in a decrease in the cold storage capacity, which in turn leads to a decrease in the discharge, so the energy efficiency η_{all} shows a downward trend. ΔT affects the heat exchange temperature difference and heat exchange efficiency of each heat exchanger, so when ΔT increases, UA_{all} decreases, and it can be seen that UA_{all} decreases faster when the heat exchange temperature difference increases within 1~5 °C.

The result shows that smaller T_{com} and ΔT will improve the overall efficiency, but the economic performance will be negatively affected. In order to achieve better thermodynamic and thermal economic performance simultaneously, it is necessary to use an optimization algorithm to design the specific operating parameters of the system.

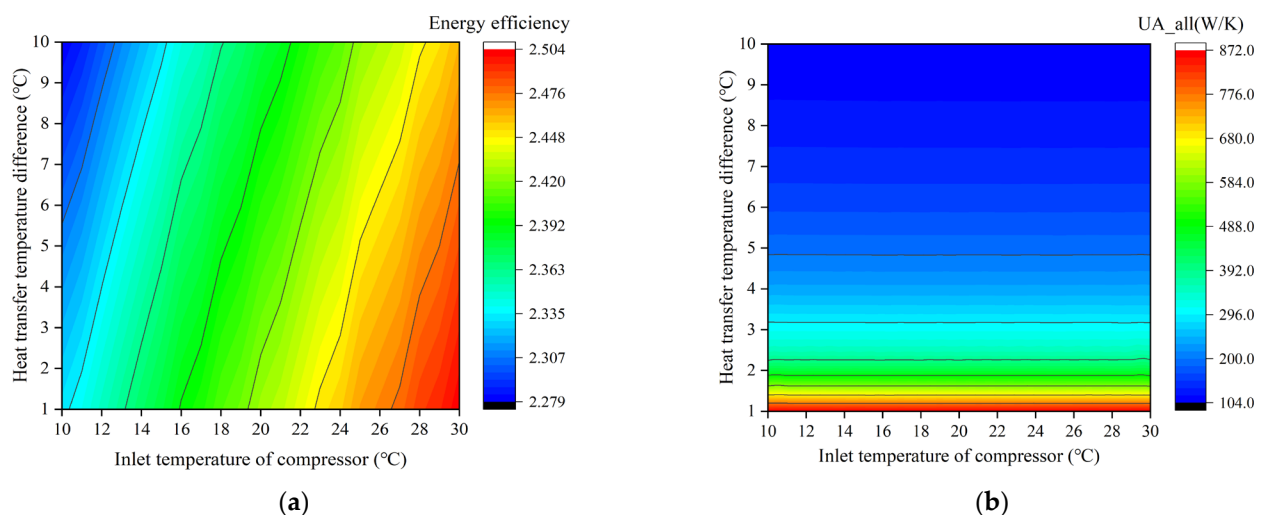


Figure 7. (a) The impact of coupling parameters on η_{all} ; (b) the impact of coupling parameters on UA_{all} .

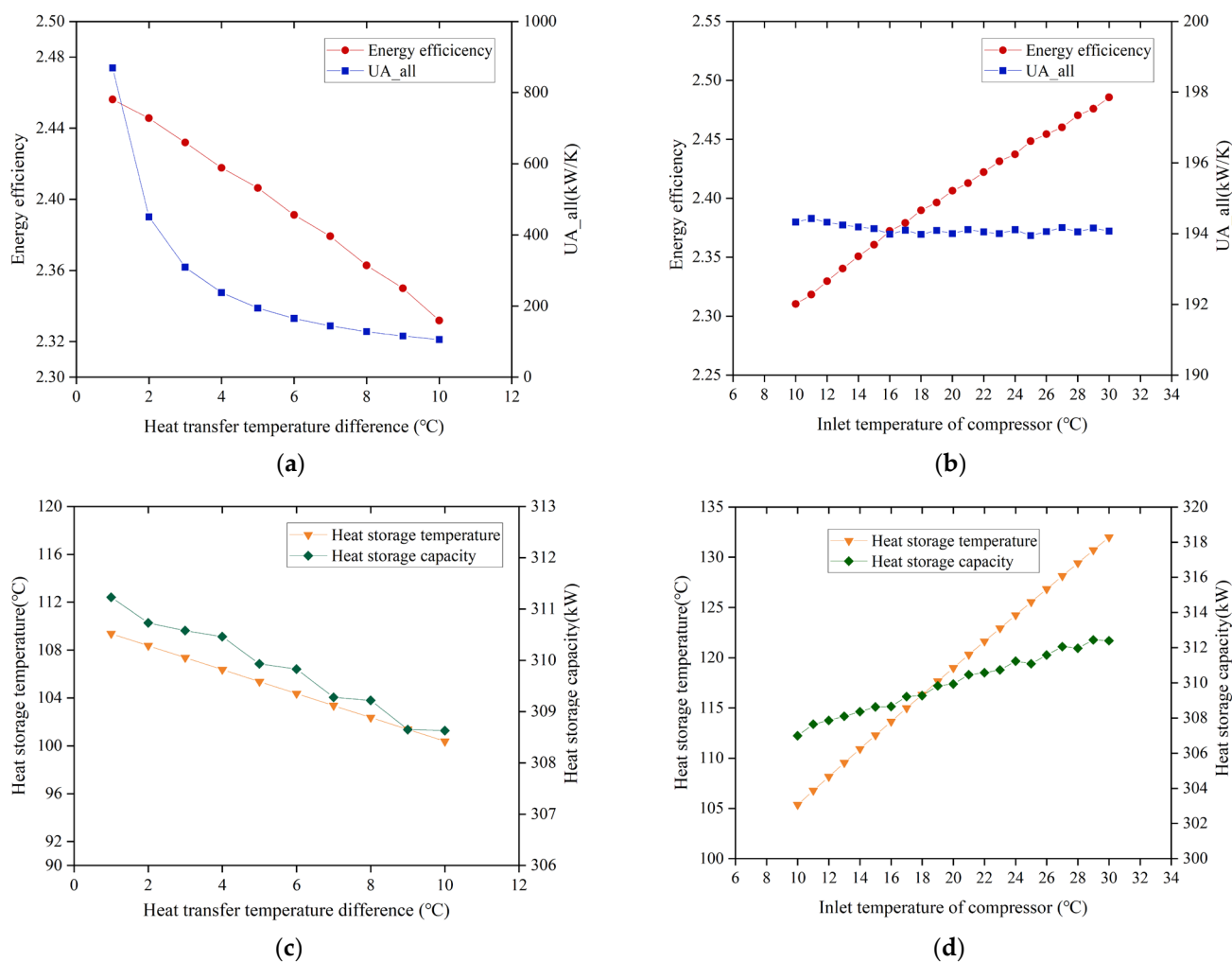


Figure 8. (a) The impact of heat transfer temperature difference on system performance; (b) the impact of inlet temperature of the compressor on system performance; (c) the impact of the heat transfer temperature difference on heat storage capacity; (d) the impact of the inlet temperature of the compressor on heat storage capacity.

4.4. Mechanical Component Efficiency of System

For a thermal system, the isentropic efficiency η_{is} of the expansion/compression components reflects the energy conversion effect. Generally speaking, the higher the isentropic efficiency η_{is} , the better the thermodynamic performance and economic performance of the system. However, in practical engineering applications, when selecting mechanical components according to the required capacity of the system, it remains to be determined which of the isentropic efficiencies of the compressor and turbine has a greater impact on the performance of the system and which should be given priority when the optimum cannot be met at the same time.

Figure 9 shows the results of system η_{all} and UA_{all} changes under different $\eta_{is,com}$ and $\eta_{is,turb}$. As expected, η_{all} increases with $\eta_{is,com}$ and $\eta_{is,turb}$, and it is easy to understand that the higher the isentropic efficiency, the better the thermodynamic performance.

It can be calculated that the isentropic efficiency of the compressor has a greater impact on the performance of the system. When the isentropic efficiency of the compressor changes by 0.1, the energy efficiency changes by 0.35 on average, while when the isentropic efficiency of the expander changes by 0.1, the energy efficiency changes by 0.27 on average. Therefore, the compressor with higher isentropic efficiency is given priority when selecting components.

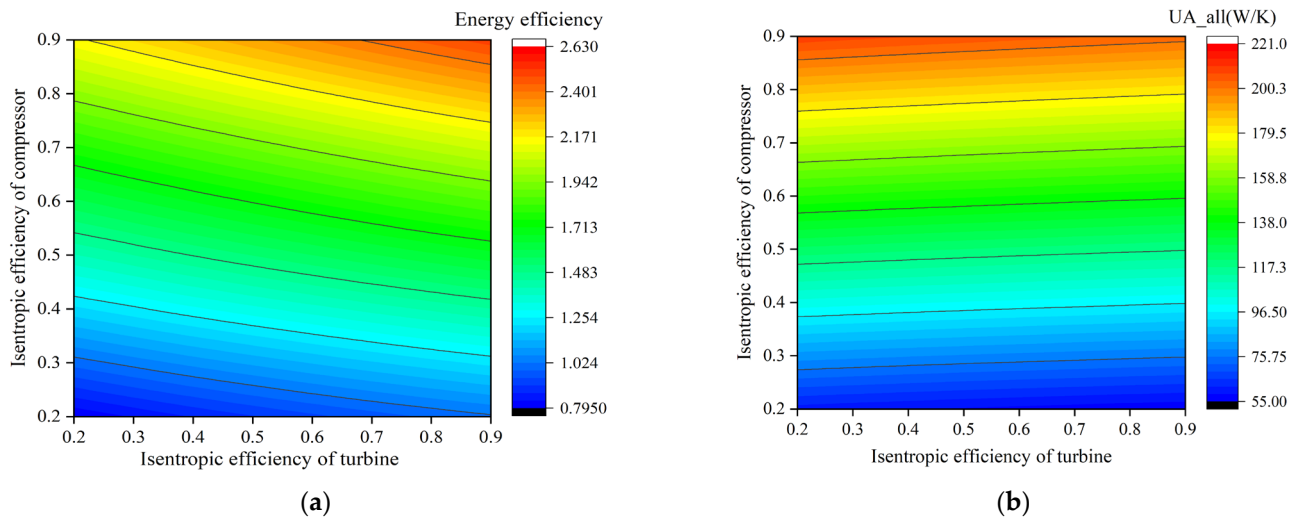


Figure 9. (a) The impact of mechanical efficiency on η_{all} ; (b) the impact of mechanical efficiency on UA_{all} .

4.5. Multi-Objective Optimization and Decision Making

The PTES system in this paper is the same as in most of the engineering problems; the optimization of thermodynamic performance is a multi-objective optimization problem, and in most cases, an improvement in one index may mean a reduction in other indexes. It is almost impossible to achieve the optimal of multiple indexes at the same time. It is difficult to decide the only optimal solution; instead, coordination and compromise are made between them to make the overall goal as optimal as possible. Therefore, it is necessary to find the Pareto solution set through multi-objective optimization and to find a satisfactory solution through multi-objective decision so as to guide the setting of the system operating parameters.

Since η_{all} and UA_{all} show opposite trends, it is almost impossible to achieve the optimal for both at the same time. Therefore, η_{all} and UA_{all} are considered to adopt a multi-objective optimization algorithm to make the overall objective as optimal as possible. A multi-objective genetic algorithm optimization with energy efficiency η_{all} and UA_{all} as the optimization objectives is considered. For the multi-objective genetic algorithm optimization problem, the Pareto front method of genetic algorithm (GA) is adopted [25] to achieve the optimal scheme of balancing the energy utilization rate and total UA value. The mathematical model of the optimization is shown in Equation (28):

$$f(P_{hp}, T_{eva}, P_{he}, T_{cond}, T_{comp}, \Delta T) = \{max\eta_{all}, minUA_{all}\} \quad (28)$$

After the completion of the multi-objective optimization, the Pareto front of the objective function is generated, which contains multiple individuals [26,27]. In order to select the best individual, the TOPSIS decision-making method is used [28]. The TOPSIS method is a commonly used method in multi-objective decision analysis. Its basic method is to find out the ideal solution of each standardized objective function, judge the approximation degree of each configuration scheme and the ideal solution, and then sort the final scheme according to it. It was first proposed by C.L. Hwang and K. Yoon in 1981 [29]. Firstly, the index evaluation matrix was established for the optimized population, and then the matrix was normalized. The obtained population matrix was shown as follows:

Energy efficiency	Total UA value
X_1	Y_1
X_2	Y_2
\dots	\dots
X_n	Y_n

The data in the matrix are normalized, and the processing process is shown in Equations (29) and (30):

$$X'_i = \frac{X_i}{\sqrt{X_1^2 + X_2^2 + \dots + X_n^2}} \tag{29}$$

$$Y'_i = \frac{Y_i}{\sqrt{Y_1^2 + Y_2^2 + \dots + Y_n^2}} \tag{30}$$

The normalized matrix is as follows:

Energy efficiency	Total UA value
X'_1	Y'_1
X'_2	Y'_2
\dots	\dots
X'_n	Y'_n

The ideal solution refers to the combination of the maximum values of two indexes selected from the normalized matrix, and the non-ideal solution is a combination of the minimum values of two indexes selected from the normalized matrix. The calculation equations for the ideal and non-ideal solutions are shown in Equations (31) and (32), respectively:

$$(X'_{max}, Y'_{max}) = \max(X'_i, Y'_j) \tag{31}$$

$$(X'_{min}, Y'_{min}) = \min(X'_i, Y'_j) \tag{32}$$

The equations for calculating the distance between each group of numbers in the matrix after normalization and the ideal solution and the non-ideal solution are shown in Equations (33) and (34), respectively:

$$L_{max} = \sqrt{(X'_i - X'_{max})^2 + (Y'_i - Y'_{max})^2} \tag{33}$$

$$L_{min} = \sqrt{(X'_i - X'_{min})^2 + (Y'_i - Y'_{min})^2} \tag{34}$$

The evaluation indexes of the TOPSIS decision method are shown in Equation (35):

$$M = \frac{L_{max}}{L_{max} + L_{min}} \tag{35}$$

The optimal solution of the TOPSIS method is required to be closest to the positive ideal solution, while at the same time, far from the negative ideal solution. The smaller the evaluation index M of the optimized individual, the closer the individual is to the ideal solution; then, the individual is the optimal individual after GA optimization.

Genetic algebra is set to 500, population size is 100, crossover probability is 0.8, mutation probability is 0.1, and the optimal front solution set of the system is obtained through calculation.

The Pareto diagram is shown in Figure 10. The ‘‘positive ideal point’’ means the minimum value of ‘‘M’’, which indicates that the distance between the individual and the

ideal solution is the shortest. The “negative ideal point” means the maximum value of “M”, which indicates that the distance between the individual and the ideal solution is the longest. Each point in the optimal solution set is shown in the figure, and based on the energy efficiency of each point and the total UA value, the distance from the ideal solution can be calculated, and the positive and negative ideal points can be found.

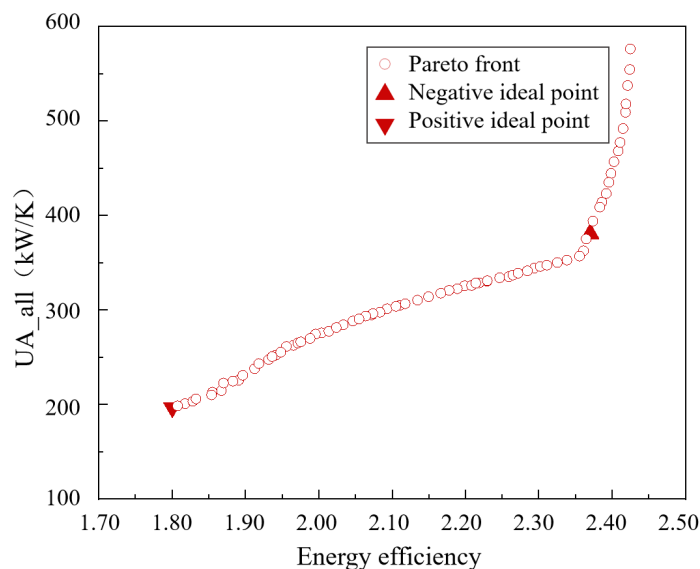


Figure 10. Pareto front of the result of multi-objective optimization.

Within the range of basic parameters set in Table 4, the optimal solution set is selected by finding solutions that meet the requirements of high energy utilization and low total UA of the heat exchanger. With the increase in energy efficiency, the total UA value also increases gradually. The optimal decision variables after the TOPSIS decision are shown in Table 5, and the performance index parameters of the system are shown in Table 6.

Table 4. Parameters of multi-objective optimization algorithm.

Parameter	Physical Meaning	Value Range
P_{hp}	High pressure of heat pump	12~20 MPa
T_{eva}	Evaporating temperature of heat pump	-5~15 °C
P_{he}	High pressure of heat engine	12~20 MPa
T_{cond}	Condensing temperature of heat pump	10~30 °C
T_{com}	Inlet temperature of compressor	10~30 °C
ΔT	Heat transfer temperature difference	1~10 °C

Table 5. Results of multi-objective optimization decision making.

Parameter	Physical Meaning	Optimal Value
P_{hp}	High pressure of heat pump	16.1 MPa
T_{eva}	Evaporating temperature of heat pump	-0.12 °C
P_{he}	High pressure of heat engine	12.2 MPa
T_{cond}	Condensing temperature of heat pump	10.7 °C
T_{com}	Inlet temperature of compressor	15.08 °C
ΔT	Heat transfer temperature difference	3.1 °C

Table 6. System performance of multi-objective optimization decision making.

Energy Efficiency	Total UA Value	Thermal Storage Capacity	Cold Storage Capacity	Thermal Storage Temperature	Cold Storage Temperature	Output Electricity
2.39	357.4 W/K	38.2 kW	195.8 kW	136.9 °C	2.2 °C	37.7 kW

The data of system performance analysis are used precisely to provide the basis and parameter design range for system optimization. In the final selection of the optimal solution, the selection principle is to select the solution closest to the ideal point as the optimal solution in the optimal solution set selected by the algorithm. The optimization scheme not only can meet the requirements of thermal performance and thermal economic performance but also be the most suitable for system operation within the set parameter range. The optimal solution selected according to the TOPSIS decision-making method can reflect the working condition of each point of the system when the thermodynamic and thermal economic performances of the system are relatively excellent, which is an optimal condition of the PTES system. It provides a pattern for the optimal working condition design and practical application of the multiple energy storage system.

5. Conclusions

Based on the application prospect of CO₂ PTES in the field of renewable energy storage, this paper constructs a multiple energy storage system, carries out system parameter analysis and performance optimization research, and draws the following main conclusions:

- (1) Through the form of the multistage compression heat pump cycle, the PTES system achieved a cascade heat storage pattern. The system can store about 0 °C of cold capacity, used to meet the needs of the cooling load. At the same time, it can store approximately 50 °C medium-temperature hot water, used to provide domestic hot water for the user side, and store the high-temperature heat above 115 °C for driving the turbine to generate electricity. The system not only can store renewable power, but also realize the flexible regulation of storage/release of power and meet the demand of multiple loads of heating and cooling in different periods.
- (2) Through the comprehensive analysis of the key parameters of the system, it is found that the effect of the heat pump parameters on the system performance is greater than that of the heat engine parameters. When $P_{hp} = 12$ MPa and $T_{eva} = -5$ °C, the η_{all} of the system reaches the highest value of 2.43. The change trend of UA_{all} is the same as that of η_{all} , and the minimum value of UA_{all} is 61.32 kW/K when $P_{hp} = 20$ MPa and $T_{eva} = 15$ °C are used. However, η_{all} and UA_{all} do not show a simple linear relationship with the change in heat engine parameters.
- (3) The genetic algorithm is used to realize the comprehensive optimization of the PTES system. In addition, the optimal solution of the Pareto front solution set is obtained by the TOPSIS decision-making method. The optimal energy efficiency of the system is 2.39, and the total UA value is 357.4 kW/K.

The results obtained in this paper can provide a basis for parameter analysis and performance optimization of CO₂ PTES and provide ideas and schemes for renewable energy storage and diversified utilization.

6. Future Work

The energy storage system combining cold, heat, and power generation proposed in this article is a multistage compression heat pump energy-storage system based on the basic principle of the PTES system. In addition to the traditional electrothermal conversion ability, it also has the function of coupling multiple heat sources and providing multistage heat energy. Although PTES is a system-level concept, some technical challenges relating to materials and components remain to be overcome, and there are currently few related system experiments and landing engineering projects. Therefore, it is worth exploring to study the running performance and components of the system. Our future work will focus on the establishment and testing of the test bed as well as the evaluation of operational performance and overall optimization.

Author Contributions: Conceptualization, Y.Y.; methodology, Y.W.; software, Y.W.; validation, Y.W.; investigation, Y.W.; resources, Z.K.; data curation, Y.W.; writing—original draft preparation, Y.W.; writing—review and editing, J.F.; visualization, Y.W.; supervision, Y.W. All authors have read and agreed to the published version of the manuscript.

Funding: This research received no external funding.

Data Availability Statement: Data available upon request.

Conflicts of Interest: The authors declare no conflicts of interest.

Nomenclature

h	Specific enthalpy, kJ/kg
m	Mass flow rate, kg/s
W_C	Input electric power, kW
W_{out}	Output electric power, kW
Q	Heat rate, kW
T	Temperature, °C
Greek Symbols	
ΔT	Temperature difference, K
η_{is}	Isentropic efficiency of mechanical components
η_{all}	Energy efficiency of the system
η_{he}	Thermodynamic efficiency of the heat engine
Subscripts	
hp	Heat pump
he	Heat engine
$com; C$	Compressor
$cool$	Cooling capacity
hot, m	Medium-temperature water
hot, h	High-temperature water
eva	Evaporator
$cond$	Condenser
Abbreviations	
PTES	Pumped thermal energy storage
UA	Heat exchanger performance

References

1. Bp. Energy Outlook. Available online: <https://www.bp.com/en/global/corporate/energy-economics/energy-outlook.html> (accessed on 1 October 2024).
2. Rostirolla, G. A Survey of Challenges and Solutions for the Integration of Renewable Energy in Datacenters. *Renew. Sustain. Energy Rev.* **2022**, *155*, 111787. [CrossRef]
3. Wang, S. Economic Study on the Application of Energy Storage in Regional Electricity Market System. Ph.D. Thesis, University of Chinese Academy of Sciences, Beijing, China, 2021.
4. Erixno, O.; Rahim, N.A.; Ramadhani, F.; Adzman, N.N. Energy Management of Renewable Energy-Based Combined Heat and Power Systems: A Review. *Sustain. Energy Technol. Assess.* **2022**, *51*, 101944. [CrossRef]
5. He, Z.; Qi, W.; Song, J.; Cui, S.; Li, H. The thermodynamic analysis of a liquefied air energy storage system coupled with liquefied natural gas. *Energy Storage Sci. Technol.* **2020**, *10*, 1589–1596.
6. Liang, T.; Vecchi, A.; Knobloch, K.; Sciacovelli, A.; Engelbrecht, K.; Li, Y.; Ding, Y. Key Components for Carnot Battery: Technology Review, Technical Barriers and Selection Criteria. *Renew. Sustain. Energy Rev.* **2022**, *163*, 112478. [CrossRef]
7. Novotny, V.; Basta, V.; Smola, P.; Spale, J. Review of Carnot Battery Technology Commercial Development. *Energies* **2022**, *15*, 647. [CrossRef]
8. Saher, S.; Johnston, S.; Esther-Kelvin, R.; Pringle, J.M.; MacFarlane, D.R.; Matuszek, K. Trimodal Thermal Energy Storage Material for Renewable Energy Applications. *Nature* **2024**, *636*, 622–626. [CrossRef]
9. Dumont, O. Carnot Battery Technology: A State-of-the-Art Review. *J. Energy Storage* **2020**, *32*, 101756. [CrossRef]

10. Strasser, M.N. A Cost and Performance Comparison of Packed Bed and Structured Thermocline Thermal Energy Storage Systems. *Sol. Energy* **2014**, *108*, 390–402. [[CrossRef](#)]
11. Zhang, Q.; Wang, L.; Xu, Y.; Chen, H. Research progress in pumped heat electricity storage system: A review. *Proc. CSEE* **2018**, *38*, 178–185.
12. Wang, L. Unbalanced Mass Flow Rate of Packed Bed Thermal Energy Storage and Its Influence on the Joule-Brayton Based Pumped Thermal Electricity Storage. *Energy Convers. Manag.* **2019**, *185*, 593–602. [[CrossRef](#)]
13. Mercangöz, M. Electrothermal Energy Storage with Transcritical CO₂ Cycles. *Energy* **2012**, *45*, 407–415. [[CrossRef](#)]
14. Morandin, M. Conceptual Design of a Thermo-Electrical Energy Storage System Based on Heat Integration of Thermodynamic Cycles—Part A: Methodology and Base Case. *Energy* **2012**, *45*, 375–385. [[CrossRef](#)]
15. Morandin, M. Conceptual Design of a Thermo-Electrical Energy Storage System Based on Heat Integration of Thermodynamic Cycles—Part B: Alternative System Configurations. *Energy* **2012**, *45*, 386–396. [[CrossRef](#)]
16. Morandin, M. Thermo-economic Design Optimization of a Thermo-Electric Energy Storage System Based on Transcritical CO₂ Cycles. *Energy* **2013**, *58*, 571–587. [[CrossRef](#)]
17. Carro, A.; Chacartegui, R.; Ortiz, C.; Carneiro, J.; Becerra, J.A. Energy Storage System Based on Transcritical CO₂ Cycles and Geological Storage. *Appl. Therm. Eng.* **2021**, *193*, 116813. [[CrossRef](#)]
18. Benato, A. Heat Transfer Fluid and Material Selection for an Innovative Pumped Thermal Electricity Storage System. *Energy* **2018**, *147*, 155–168. [[CrossRef](#)]
19. Sun, P. Design and Application of Pumped Thermal Energy Storage System Based on High and Low Temperature Energy Storage. Master's Thesis, Zhejiang University, Hangzhou, China, 2023.
20. Laterre, A.; Dumont, O.; Lemort, V.; Contino, F. Is Waste Heat Recovery a Promising Avenue for the Carnot Battery? Techno-Economic Optimisation of an Electric Booster-Assisted Carnot Battery Integrated into Different Data Centres. *Energy Convers. Manag.* **2024**, *301*, 118030. [[CrossRef](#)]
21. Kasaeian, A. Solar-Driven Polygeneration Systems: Recent Progress and Outlook. *Appl. Energy* **2020**, *264*, 114764. [[CrossRef](#)]
22. Yu, L.; Zhu, Y.; Wu, Y. *Medium and Low Temperature Waste Heat Power Generation Technology*, 1st ed.; Shanghai Jiao Tong University Press: Shanghai, China, 2015; pp. 123–125.
23. Kim, Y.-M.; Shin, D.-G.; Lee, S.-Y.; Favrat, D. Isothermal Transcritical CO₂ Cycles with TES (Thermal Energy Storage) for Electricity Storage. *Energy* **2013**, *49*, 484–501. [[CrossRef](#)]
24. Hu, S.; Yang, Z.; Li, J.; Duan, Y. Thermo-Economic Analysis of the Pumped Thermal Energy Storage with Thermal Integration in Different Application Scenarios. *Energy Convers. Manag.* **2021**, *236*, 114072. [[CrossRef](#)]
25. Deb, K.; Pratap, A.; Agarwal, S.; Meyarivan, T. A Fast and Elitist Multiobjective Genetic Algorithm: NSGA-II. *IEEE Trans. Evol. Comput.* **2002**, *6*, 182–197. [[CrossRef](#)]
26. Nondy, J. Exergoeconomic Investigation and Multi-Objective Optimization of Different ORC Configurations for Waste Heat Recovery: A Comparative Study. *Energy Convers. Manag.* **2021**, *245*, 114593. [[CrossRef](#)]
27. Yu, X. Sensitivity Analysis of Thermophysical Properties on PCM Selection under Steady and Fluctuating Heat Sources: A Comparative Study. *Appl. Therm. Eng.* **2021**, *186*, 116527. [[CrossRef](#)]
28. Wang, L.; Bu, X.; Li, H. Multi-Objective Optimization and off-Design Evaluation of Organic Rankine Cycle (ORC) for Low-Grade Waste Heat Recovery. *Energy* **2020**, *203*, 117809. [[CrossRef](#)]
29. Hwang, C.; Yoon, K. *Multiple Attribute Decision Making: Methods and Applications*; Springer: New York, NY, USA, 1981.

Disclaimer/Publisher's Note: The statements, opinions and data contained in all publications are solely those of the individual author(s) and contributor(s) and not of MDPI and/or the editor(s). MDPI and/or the editor(s) disclaim responsibility for any injury to people or property resulting from any ideas, methods, instructions or products referred to in the content.